Soil moisture profile estimation under bare and vegetated soils using combined L-band and P-band radiometer observations: An incoherent modeling approach

Foad Brakhasi, Jeffrey P Walker, Jasmeet Judge, Pang-Wei Liu, Xiaoji Shen, Nan Ye, Xiaoling Wu, In-Young Yeo, Edward Kim, Yann H. Kerr, et al.

Soil moisture profile estimation under bare and vegetated soils using combined L-band and P-band radiometer observations: An incoherent modeling approach

Foad Brakhasi[a, □], Jeffrey P. Walker[a], Jasmeet Judge[b], Pang-Wei Liu[c], Xiaoji Shen[d], Nan Ye[a], Xiaoling Wu[a], In-Young Yeo[e], Edward Kim[c], Yann Kerr[f], and Thomas Jackson[g]

[a] Department of Civil Engineering, Monash University, Clayton, Australia

[b] Department of Agricultural and Biological Engineering, University of Florida, Gainesville, USA

[c] Hydrological Sciences Branch, NASA Goddard Space Flight Center, Greenbelt, USA

[d] Yangtze Institute for Conservation and Development, Hohai University, Nanjing, China

[e] School of Engineering, The University of Newcastle, Callaghan, Australia

[f] Centre d'Etudes Spatiales de la Biosphère, Toulouse, France

[g] USDA ARS Hydrology and Remote Sensing Laboratory (Retired), Beltsville, USA

[*] *Corresponding author.*

E-mail addresses: foad.brakhasi@monash.edu, brakhasi.f@gmail.com.

ABSTRACT

Understanding the distribution of moisture throughout the soil profile is crucial for effective water management in the field of agriculture. This knowledge enables farmers and water managers to make informed decisions regarding the timing and amount of irrigation needed to optimize crop growth. To estimate the soil moisture profile, this study utilized L-band and P-band radiometry with three multilayer incoherent models, based on a zero-order (IZ), first order (IF), and incoherent solution (IS) approximation, as well as the conventional tau-omega (TO) model. The result of these models was also compared with the coherent model results published by Brakhasi et al. (2023). Two mathematical shape functions - linear (Li) and second-order polynomial (Pn2) - were used to represent the soil moisture profile. Observations from a tower-based experiment were used under different land cover conditions, namely bare, bare-weed, grass, wheat, and corn. The Root Mean Square Error (RMSE) was calculated between the observed and estimated soil moisture profiles, with the results indicating that RMSE values were similar for all four radiative transfer models, with the Pn2 function outperforming the Li function in deeper layers. The multilayer incoherent models generated slightly better results than the conventional TO model, particularly for the shallow layers, but their complexity was not justified for the small gain in performance. Additionally, the comparison between conventional and multi-layer incoherent models with stratified coherent Njoku model was reveal that the latter slightly outperformed the formers under dry bare soil condition. The conventional TO model provided an average profile estimation depth ranging from 1cm (under corn) to 39cm (under bare), depending on the soil moisture profile gradient and value in the shallow layers. These findings pave the way for estimating soil moisture profile on a global scale using combined L-band and P-band radiometry from future satellite missions operating at these two bands.

Keywords: Soil moisture profile, P-band, L-band, Incoherent, tau-omega, Estimation depth

1. Introduction

Soil moisture information is a must for all important ecological aspects and plays a critical role in all physiological processes (Swaroop Meena and Datta, 2021). From a hydrological perspective it is a small fraction (0.05%) of the freshwater globally (2.5%). However, its importance to water, energy, and carbon cycles and the distribution of precipitation far surpasses its physical amount (Oki and Kanae, 2006; Robinson et al., 2008). It is highly variable both in space, especially in the top 20cm of the soil (Shi et al., 2014), and time, due to variability in precipitation (Schoener and Stone, 2020; Manoj et al., 2022), vegetation, and soil texture (Baroni et al., 2013). The roots of major agricultural crops with the highest density are found at depths of 20cm or less, according to Haberle and Svoboda (2015). Lack of adequate soil moisture in this region can therefore restrict plant growth and crop yield (Svoboda, P. et al., 2020), thereby impacting food security (Sadri et al., 2020). In a study conducted by Ma et al (2023), the effects of surface drip irrigation and direct root-zone irrigation on the productivity of grapevine and berry were compared. The results revealed that the implementation of direct root-zone irrigation substantially improved the crop productivity and quality of Chardonnay grapes by 23 – 34%, while also reducing the necessary irrigation amount by 16 – 23%.

Passive microwave remote sensing is a well-accepted technique for estimation of soil moisture, with the two current missions of SMOS (Soil Moisture and Ocean Salinity) and SMAP (Soil Moisture Active Passive) operating at L-band (~ 21cm wavelength). However, they are limited to estimating soil moisture in the top ~ 5cm of the soil column. Currently there are eight global root zone soil moisture products, including GLDAS NOAH, ERA-5, MERRA-2, NCEP R1, NCEP R2, JRA-55, SMAP level 4 and SMOS level 4, which are derived by model-based simulations sometimes combined with the shallow soil moisture observations from satellite. But the accuracy of these products is highly dependent on several

factors, such as the forcing data, model structure and parameterization, data assimilation method and assimilated variables (Xu et al., 2021).

The advent of P-band radiometry presents a novel opportunity for the remote sensing community, enabling the investigation of soil moisture at deeper layers. Having a wavelength of approximately 40cm, means that emissions can be observed from deeper in the soil than other frequencies (Shen et al., 2020), such as L-band, and are also comparatively less susceptible to interference from vegetation and surface roughness (Shen et al., 2022a, 2022b). By integrating L-band and P-band signals, emanating from different depths of the soil, it is expected that soil moisture can be estimated beyond the extent of each frequency individually. Accordingly, Brakhasi et al. (2023a) successfully estimated the soil moisture profile using a multilayer coherent approach through the utilization of combined L-band and P-band radiometry on bare soil. Upon implementation of a second-order polynomial (linear) profile shape function, the outcome yielded 28cm(20cm) and 5cm(5cm) as the respective soil moisture profile estimation depths during dry and wet periods respectively.

The estimation of soil moisture variation within the profile from microwave observations becomes increasingly complex when there is a layer of vegetation present on the surface, as opposed to barren soil conditions. Furthermore, in comparison to incoherent models, coherent models are more computationally intensive, yet their accuracy in estimated brightness temperature is comparable to that of incoherent models (Brakhasi et al. 2023b). Additionally, the linearity of soil moisture at depths of less than 30cm potentially allows for the utilization of the conventional Tau Omega model as a replacement for multilayer incoherent models. Therefore, this study assessed the multi-frequency soil moisture profile estimation capability using combined L- and P-band with incoherent models under conditions of bare, bare-weed, grass, wheat and corn.

2. **Experimental Data**

This study is based on radiometric measurements acquired from a tower-based experiment established from December 2017 to June 2022 at Coral Lynn, Victoria, Australia (Brakhasi et al, 2023b). The tower carrying two radiometers, namely PLMR (Polarimetric L-band Multi-beam Radiometer) and PPMR (Polarimetric P-band Multi-beam Radiometer), was at the center of a paddock (150m×150m). The paddock was divided into four quadrants and managed with different conditions in terms of surface roughness and vegetation. For this study, a variety of land surface conditions are explored, including dry and wet profiles under two different bare soil periods (2nd to 30th April 2019, 3rd to16th March 2020), one bare soil with weeds (18th November 2020 to 8th December 2020), one grass (1st to 27th March 2018), one wheat (1st to 23rd December 2018), and one corn (20th December 2020 to 4th March 2021) with very low to high vegetation water contents (VWC from 0.5 to 22 kg/m^3).

The dataset includes brightness temperature at L- and P-band frequencies at an incidence angle of ~ 40°, soil moisture and soil temperature profile measurements at ground stations installed at the border of the quadrants from the surface to a depth of 60cm in 5cm increments, and weekly measurements of VWC and surface roughness. The radiometer was calibrated weekly using cold/warm targets, and the representativeness of the ground stations were investigate using weekly near-surface soil moisture measurements (~5cm) by the Hydra-probe Data Acquisition System (HDAS; Merlin et al., 2007). The composition of the soil texture, at an average depth of 0 to 60cm, is made up of 18.3% clay, 13.7% sand, and 68% silt. This composition indicates a silty loam type, with a surface layer having a bulk density of 0.87 kg/m^3.

The shapes of the soil moisture profile observed at the ground stations are presented in Fig. 2 for the periods investigated in this study. It is evident that the surface soil moisture has a higher degree of variation compared to the bottom soil moisture in most cases, except during

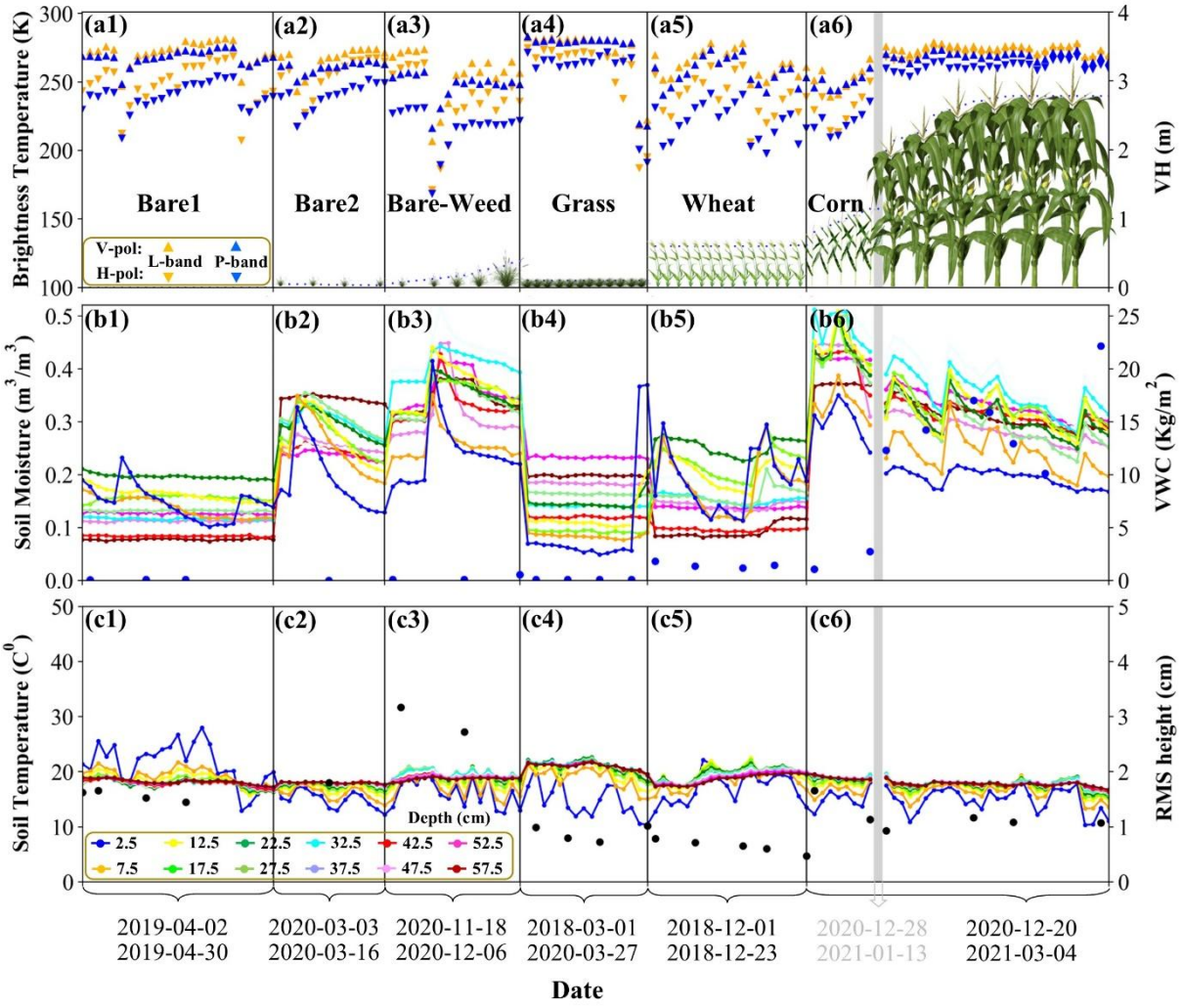

Fig. 1. Collected data over six periods including bare, grass, wheat, and corn conditions: a) TB observations from PLMR and PPMR instruments at 6 AM and PM; b) station time-series soil moisture; and c) station time-series soil temperature. The vegetation height (VH), vegetation water content (VWC) and RMS height are plotted as a secondary axis on the brightness temperature, soil moisture and soil temperature profile plots respectively. The gray area in the corn period is a 17-day gap where the tower was lowered due to unscheduled maintenance.

the corn period. Interestingly, the soil moisture at a depth of 15 to 40cm exhibits a higher degree of variability than the surface and bottom soil moisture during the corn period. During the bare period with weeds (bare-weed), the surface soil moisture shows a greater degree of variability than the deeper layer, although some variability is still observed. Notably, during the second bare period (bare2), as the depth increased, the variability of soil moisture

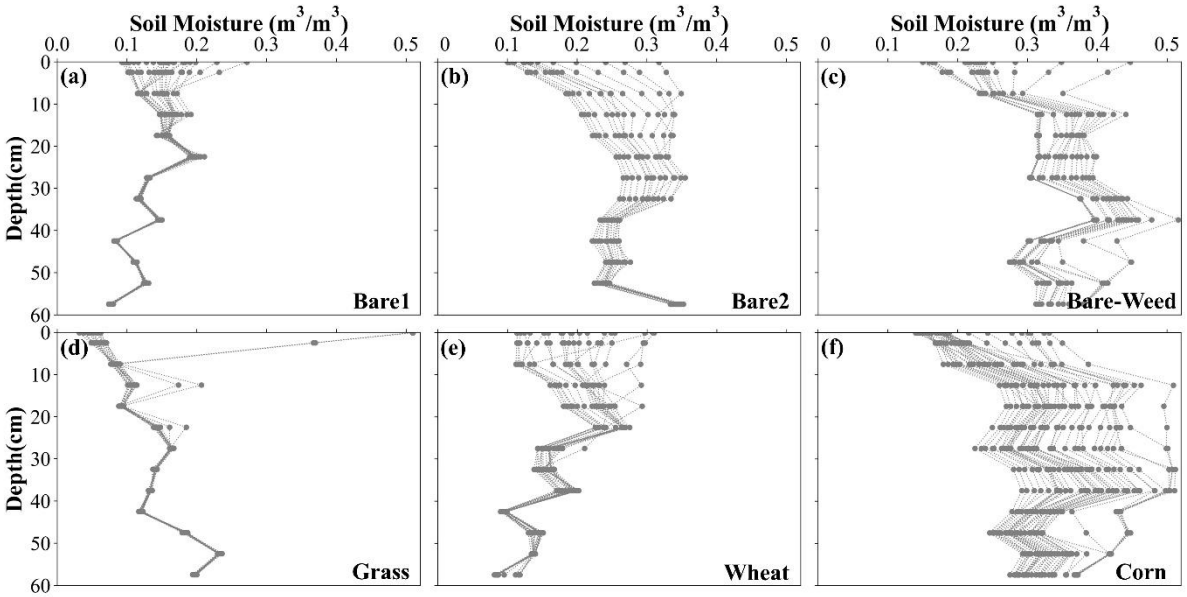

Fig. 2. Shape of the soil moisture profile (one profile per day) under different land cover conditions including a) bare1, b) bare2, c) bare-weed, d) grass, e) wheat, and f) corn.

decreased. During the first bare period (bare1), grass and wheat periods, the variability of soil moisture was observed to be mainly below 25cm. Low soil moisture values were noted throughout the grass period with the exception being a heavy rainfall event towards the end, resulting in a wet soil moisture profile with a high gradient in the shallow layer. Overall, these observations provide important insights into the distribution and variability of soil moisture across the different periods and depths.

3. Methodology

The goal of this study is to investigate the performance of the incoherent models for estimating soil moisture profile variation using combined L-band and P-band radiometer observations. Furthermore, these models will be evaluated in comparison to the performance of the stratified coherent Njoku model utilized by Brakhasi et al. (2023). Estimating soil moisture throughout the profile allows for a more detailed understanding of the distribution and availability of water in the soil, which can inform irrigation and water management decisions, as well as predictions of crop yield and water use efficiency. Additionally, monitoring soil moisture at different depths can provide insight into the movement of water

through the soil and the dynamics of the water cycle in a given area. In this study, the performance of four different incoherent models is compared, including the conventional tau-omega model and three multilayer incoherent models based on zero-order, first order and incoherent solution approximation of volume scattering inside the soil, to determine which is most effective at estimating the soil moisture profile.

3.1 Radiative transfer models

The soil moisture content of a near-surface layer of soil can be estimated by utilizing a microwave emission model that converts brightness temperature observations from a microwave radiometer to soil moisture. Almost all of the efforts from the early 1970s to 1990s were concentrated on developing, verifying and improving the basic microwave emission models for smooth and rough soils (i.e. Mo et al., 1982; Njoku, 1976; Stogryn, 1970; Wilheit, 1978) using the data acquired from some controlled field campaigns including ground-based (by a flatbed truck or a mobile tower; Lee, 1974; Wang et al., 1982) and airborne (by an airplane or a helicopter; Ferrazzoli et al., 1992; Paloscia et al., 1993).

From these investigations, baseline approaches to account for three major variables; physical temperature, surface roughness and vegetation water content, were developed. These advances resulted in the current form of the radiative transfer equation that has been applied to vegetative conditions (the tau-omega model; Mo et al., 1982), which serves as the basis for almost all operational retrieval algorithms, including those used by the SMOS and SMAP missions (Entekhabi et al., 2014; Kerr et al., 2012; Mladenova et al., 2014; Wigneron et al., 2007). The conventional tau-omega model is a is a zero-order solution of the radiative transfer equations which assumes that the scattering phase matrix term can be neglected. Mathematically, brightness temperature at the top of vegetation (TB_{TOV}) can be estimated from the tau-omega model by

$$TB_{TOV,P=}T_{eff}(1-r_P)\Gamma_P + T_c(1-\omega_P)(1-\Gamma_P)(1+r_P\Gamma_P) + TB^{Sky\_down}r_P{\Gamma^2}_P, \quad (1)$$

where TB^{Sky_down} is the downward atmospheric contribution calculated to be to 5.3K and 13.9K at L-band and P-band respectively (ITU, 2015), and T_{eff} is the effective physical temperature of the soil layer (K). When the soil temperature is non-uniform over the radiative emission depths the temperature is considered as an "effective" temperature (weighted average over the emission path). This is particularly important at lower frequencies which can penetrate into a deeper layer of the soil and has a greater sensing depth. Wigneron et al. (2008) developed a simple parametrization for this variable using just the surface temperature (T_{surf} in Kelvin) and the deep-soil temperature (T_{deep} in Kelvin) such that

$$T_{eff} = T_{deep} + \left(T_{surf} - T_{deep}\right) \times (\mathrm{sm} \,/\, T_{surf}\omega_0)^{b_0}, \quad (2)$$

where ω_0 and b_0 depend on specific characteristics of the soil such as texture, structure and density, and were set to be 0.35 and 0.58 (Lv et al., 2014), respectively. The variable sm is the average soil moisture from the soil surface to a depth of 5cm for L-band and 7cm for P-band according to Shen et al. (2021). The variable T_c (K) is the physical temperature of the vegetation. The thermal differences between land cover types and the differences between canopy and soil temperatures is typically a minimum at 6 am (Fagerlund et al., 1970; Jackson and Kimball, 2009), and so it has been assumed that soil surface and vegetation continuum have equal temperatures (i.e. $T_{surf} \cong T_c$) at that time.

The vegetation attenuation factor (Γ_P) and single scattering albedo (ω_P) account for the vegetation attenuation (where *P* is polarization H or V), and are dependent on vegetation water content, vegetation structure, incidence angle, frequency and polarization. Consequently, Γ_P is calculated from the optical depth of the standing vegetation ($\tau_{veg,p}$) by

$$\Gamma_P = exp\left(-\frac{\tau_{veg,p}}{cos\,\theta}\right), \quad (3)$$

where θ is the incidence angle. Moreover, Jackson and Schmugge (1991) found that $\tau_{veg,p}$ can be linearly related to VWC (kg/m^2) through

$$\tau_{veg,p} = \mathrm{b} \cdot \mathrm{VWC}, \tag{4}$$

where b is a factor which is mainly dependent on the frequency, the canopy type, and the vegetation dielectric constant. In this study, the b parameter was calibrated for L-band and P-band under grass (0.11, 0.11; by the authors from another period of the data), wheat (0.11, 0.099; Shen et al., 2022), and corn (0.094, 0.053; Shen et al., 2023) conditions, respectively. The variable ω_p is defined as the ratio of the vegetation scattering to extinction coefficient ratio, calibrated for grass (0.05, 0.05; by the authors from another period of the data), wheat (0.05, 0.134; Shen et al., 2022), and corn (0.070, 0.086; Shen et al., 2023) conditions for L-band and P-band, respectively. It worth mentioning here that all of the models used in this study ignore multiple scattering within the vegetation layer, which is considered a reasonable assumption at the (low) frequency range used for soil moisture sensing.

The variable r_P is rough surface reflectivity and is calculated from the semi-empirical approach (referred here to as the hqn model) proposed by Wang and Choudhury (1981) and further developed by Wigneron et al. (2001) such that

$$r_P = \left[(1 - q_P) r^*{}_P + q_P r^*{}_Q \right] exp\left(-h_P cos^{n_P}(\theta)\right), \tag{5}$$

where $r^*{}_P$ is the smooth surface reflectivity (with $P = H$ and Q=V or $P = V$ and Q=H) and calculated for H (Eq.6) and V (Eq.7) polarizations by the Fresnel equations

$$r^*{}_H = \left| \frac{\cos(\theta) - \sqrt{\varepsilon_r - \sin^2(\theta)}}{\cos(\theta) + \sqrt{\varepsilon_r - \sin^2(\theta)}} \right|^2 \tag{6}$$

$$r^*{}_V = \left| \frac{\varepsilon_r \cdot \cos(\theta) - \sqrt{\varepsilon_r - \sin^2(\theta)}}{\varepsilon_r \cdot \cos(\theta) + \sqrt{\varepsilon_r - \sin^2(\theta)}} \right|^2, \tag{7}$$

where $\varepsilon_r = \varepsilon_r' - i \cdot \varepsilon_r''$ is the relative soil dielectric constant which includes real ($'$) and imaginary ($''$) parts. Using this model h_P accounts for the intensity of the roughness effects and is calculated using the formulation of Wigneron et al. (2001)

$$h_P = 1.3972 * \left(\frac{rms}{lc}\right)^{0.5879}, \tag{8}$$

where rms and lc are the RMS surface roughness height and correlation length as measured in the field, q_P is a polarization decoupling factor set to zero for both L- and P- bands, while n_P accounts for multi-angular and dual-polarization measurements and was calibrated to another period of the data and set to -0.50 (1.80) and -0.333 (0.415) at H (V) polarizations for L-band and P-band respectively.

A stratified incoherent radiative transfer model was introduced by Stogryn (1970) to obtain approximate values of brightness temperature for media in which the dielectric constant profile is slowly-varying and in which the absorption is small. The model is fairly straightforward to implement and an assumption is made that the imaginary part of ε_r'' is small such that $\varepsilon_r'' << \varepsilon_r'$. Their model is based on a zero-order radiative transfer approximation in which reflections at interfaces are ignored (Ulaby et al., 1986) such that

$$\mathrm{TB}_P = e_P \left\{ \int_{-\infty}^{0} \mathrm{T}(\mathrm{z}) \left(\frac{2\pi}{\lambda_0} \cdot \frac{\varepsilon_\mathrm{r}''(\mathrm{z})}{2\sqrt{\varepsilon_\mathrm{r}'^{(\mathrm{z})}}} \right) \exp\left[- \int_{\mathrm{z}}^{0} \alpha(\mathrm{z}')\mathrm{dz}' \right] \mathrm{dz} \right\}, \tag{9}$$

where the expression in round parentheses represents the attenuation coefficient $\alpha(z)$, the integral expression in curly brackets represents the effective temperature, and λ_0 is the free-space wavelength (m). This model is referred to as IZ throughout this paper. In the existing literature, it is also commonly known as a radiative transfer model.

Burke and Paris (1975) and Liu et al. (2013), further developed the zero-order model presented (Eq.9) to a first-order model (referred to as IF) and an incoherent solution (IS) radiative transfer model, respectively. In the IF model, a single reflection at the layer

interfaces is considered, while in the IS model, the propagation of radiance through each layer is taken into account. Detailed descriptions of these models are provided in Burke and Paris (1975) and Liu et al. (2013) and so are not repeated here. The models IZ, IF, and IS are multilayer and the number of layers and the profile depth were set to 100 and 1m respectively. It is worth mentioning here that the differences between these models is in the way that how they calculate the effective temperature. Thus, the output of these models is primarily the effective temperature so and by inserting T_{eff} into Eq.1 the brightness temperature at the top of vegetation ($TB_{TOV,P}$) accounting for surface roughness and vegetation is calculated.

These radiative transfer models require an appropriate soil dielectric model to convert soil moisture content to soil dielectric constant. Accordingly, the multi-relaxation generalized refractive mixing dielectric model of Mironov et al. (2013) was utilized, as it accounts for the interfacial (Maxwell-Wagner) relaxation of water in the soil, which is significant at P band (Zhang et al., 2020).

3.2 Soil moisture profile shape functions and inversion

In this study, the soil moisture profile was considered as unknown, while the soil temperature profile, VWC, and surface roughness were considered as known variables. Brakhasi et al. (2023) found that when approximating the soil temperature profile with a simple method that uses a trend of the profile together with a surface soil temperature measurement, there is little degradation on the result as compared with condition when soil temperature considered known. As a result, to minimize errors in soil moisture profile estimation, this variable is considered as a known parameter. From their study it was also revealed that a linear (hereafter referred to as Li; Eq.10) and a second-order polynomial function (hereafter referred to as Pn2; Eq.11) were the most representative for soil moisture profile estimation when compared with exponential, third-order polynomial, piecewise linear, simplified solution of

Richard Equation and a parametrized second-order polynomial shape functions (Brakhasi et al., 2023). According, the

soil moisture profile shape functions used herein are given as

$$\mathrm{SM}(z) = az + c \tag{10}$$

$$\mathrm{SM}(z) = az^2 + bz + c, \tag{11}$$

where z is depth (positive downward) and a, b and c are coefficients of the related function. Parameter c is the surface soil moisture while parameter a in Eq.10 represents the profile slope of the near-surface soil moisture content, whereas Eq.11 has an additional parameter b that controls the curvilinear shape of the profile. These parameters are generated in such a way that strange profile shapes cannot be formed and that change (maximum – minimum) of soil moisture value throughout the profile does not exceed 0.35m^3/m^3. The parameter boundaries of these function are shown in Table 1.

The estimation of soil moisture profile using L-band and P-band radiometry was done by employing two profile shape functions and a time series retrieval approach. The time series approach involved dividing the time series data of TB into dry down periods. During each period, the cost function's global minimum values exhibit a distinctive pattern resulting from

Table 1. The boundaries of parameters used in the mathematical functions. Parameter c is the surface soil moisture (m^3/m^3), a in equation 10 is the slope of the soil moisture profile and along with b in equation 11 represent the shape of the profile. The numbers in the brackets show the boundary [lower, upper] of each parameter.

Equation	$\boldsymbol{a}$ (-)	$\boldsymbol{b}$ (-)	$\boldsymbol{c}$ (m^3/m^3)
11	[-0.83, 0.83]	-	[0, 0.5]
12	[-1, 1]	[-1, 1]	[0, 0.5]

the temporal correlation of the soil moisture profile and are located in specific areas of the search space. As a result, it is easier to find multiple global minimum values at once rather than searching for them individually. Furthermore, the Particle Swarm Optimization (PSO; Eberhart and Kennedy, 1995) algorithm, which involves sharing information among the populations, was utilized as an optimization algorithm to invert the employed forward models. The PSO algorithm, when used in conjunction with the time series approach, proved to be more effective as it was able to utilize prior knowledge from the previous time step to determine the value for the next time step. The PSO algorithm with the parameter settings noted in Brakhasi et al. (2023) was employed to minimize the cost function

$$L(\bar{X}) = \frac{1}{N}\left[\sum_{P=H,V}\left|TB_{F,P}(\bar{X}) - TB_{F,P}\right|^2\right] + \left(\frac{\left|\mathrm{diff}(\sum_{1}^{N} sm_{60cm})\right|}{N-1} * 10\right) \quad (12)$$

to invert the above models for the soil moisture profile, where $(\bar{X})$ represents the parameters of interest (soil moisture profile shape function parameters in this study),$TB_{F,P}$ and $TB_{F,P}(\bar{X})$ are the calculated and observed TB, N is the number of observations, sm_{60cm} is the soil moisture at the bottom of the profile (depth of 60cm in this study), and P and F represent the polarization (H or V) and frequency (L or P), respectively. The invented term in round parentheses was employed to control the fluctuation of soil moisture at the bottom for the profile (here 60 cm).

4. Results and discussion

This study aimed to estimate the soil moisture profile under different land cover conditions including bare, grass, wheat, and corn using alternative incoherent models and it were also compared with the stratified coherent model results of Njoku model (NM; Njoku and Kong, 1977) employed in Brakhasi et al. (2023). To ensure a fair comparison, the results was compared to a modified version of the Brakhasi et al. (2023) approach, which incorporated a new cost function as shown in Eq.12. To achieve this, an approach based on a combination of

295 L-band and P-band radiometry was employed, utilizing the incoherent TO, IZ, IF, and IS

296 models. The cumulative Root Mean Square Error (RMSE) was then calculated between the

observed and estimated soil moisture profiles at various depths, ranging from 0-5cm to 0-60cm. The results of this study contribute to the development of a more accurate understanding of soil moisture profile estimation under varying land cover conditions, with potential implications for a range of applications in the field of agriculture and hydrology.

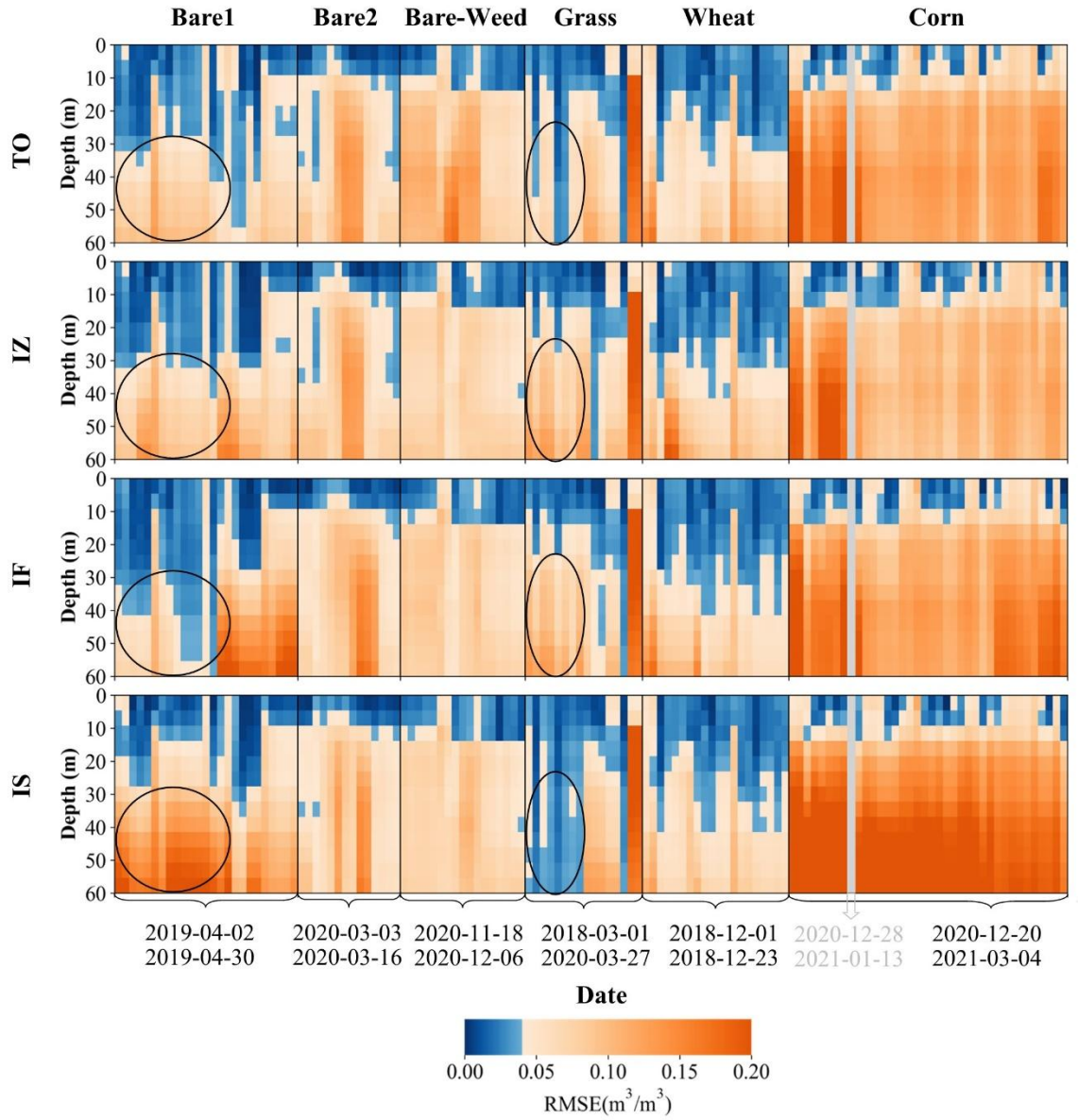

Fig. 3. Soil moisture profile estimation using combined L-band and P-band observations by utilizing the tau-omega model (TO) or a multilayer incoherent model based on zero-order (IZ), first-order (IF), or incoherent solution (IS) scattering and employing a linear profile shape function. The gray area in the corn period is a 17-day gap where the tower was lowered due to unscheduled maintenance.

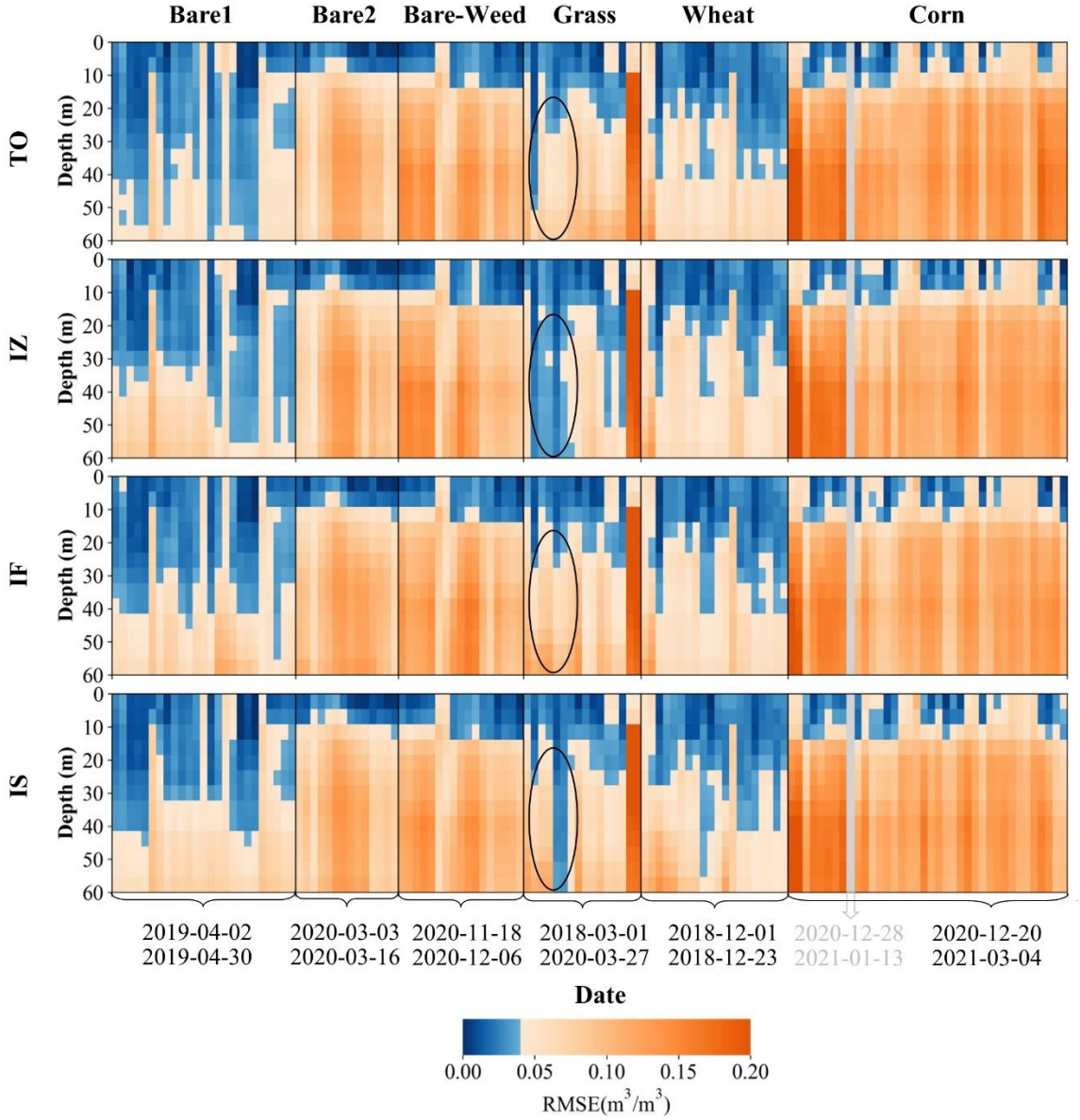

Fig. 4. Same as Fig.2 but using a second-order polynomial profile shape function.

The RMSE of the soil moisture estimate at different depths was calculated from comparing the observed and estimated soil moisture profiles obtained from the four different incoherent models. Fig. 3 and Fig. 4 present the RMSE results obtained when using the Li and Pn2 profile shape functions, respectively. The results confirmed that irrespective of the selected model, profile shape function, and the landcover conditions, the RMSE values were consistently lower for the shallow layers when compared to the deeper layers. This can be attributed to two key reasons. First, the emission contribution at L-band and P-band decreases

with increasing depth, implying that the accuracy of the estimation should also reduce with increasing soil depth due to signal loss through absorption, scattering and reflection by the soil particles. Second, the correlation between soil moisture in the surface layer and the bottom layer tends to weaken as the distance between the layers increases. Despite some differences (black ovals in Fig. 3 and Fig. 4), the outcomes of all four models were quite similar, particularly for the Pn2 profile shape function. The similarities between the results obtained from the models is relatively higher during wet periods and lower during dry periods. In particular, during dry periods, such as grass or bare periods, the L-band and P-band wavelengths carry soil moisture information of deep layers of the soil. As a result, the strength and limitations of multilayer models and mathematical functions representing the soil moisture profile become more evident. Furthermore, the average RMSE across all land cover conditions indicated that the Pn2 profile shape function outperformed the Li shape function, particularly in deeper layers (Fig. 5). This suggests that Pn2 is more robust than Li, and is able to more accurately capture the profile shape in the deeper layers. As Fig. 5 (a) illustrates, there were only minor differences in the results of the mathematical functions and models up to a depth of 12 cm. Therefore, any of these models and functions can be used if the aim is to estimate soil moisture to this depth. Moreover, it also shows that there was only slightly superior outcomes of the multilayer incoherent models IZ, IF, and IS when compared to the conventional TO model, implying that utilizing a second-order mathematical function and the conventional model yields almost identical outcomes to the more complex multilayer incoherent models. This is an important finding, as the multilayer models also require information on soil temperature throughout the entire profile, which can sometimes be difficult to obtain, while the conventional model relies on soil temperature information from just the surface and bottom layer of the profile. Irrespective of the mathematical shape functions employed, the estimation performance was inferior at deeper layers during specific

periods, namely bare2, bare-weed, the last two days of grass (following the heavy rainfall after the prolonged dry period), and corn periods. The probable cause for this could be the high levels of near-surface soil moisture reducing the depth of emissions, and the steep gradient of soil moisture in the upper layers of the soil weakening the correlation between surface and deeper soil moisture (see Fig. 1 and Fig. 2). In contrast, during bare1, grass periods (excluding the last two days), and wheat period, the soil moisture value and its gradient at the upper layer were relatively lower as compared to the other periods, leading to a greater estimation depth.

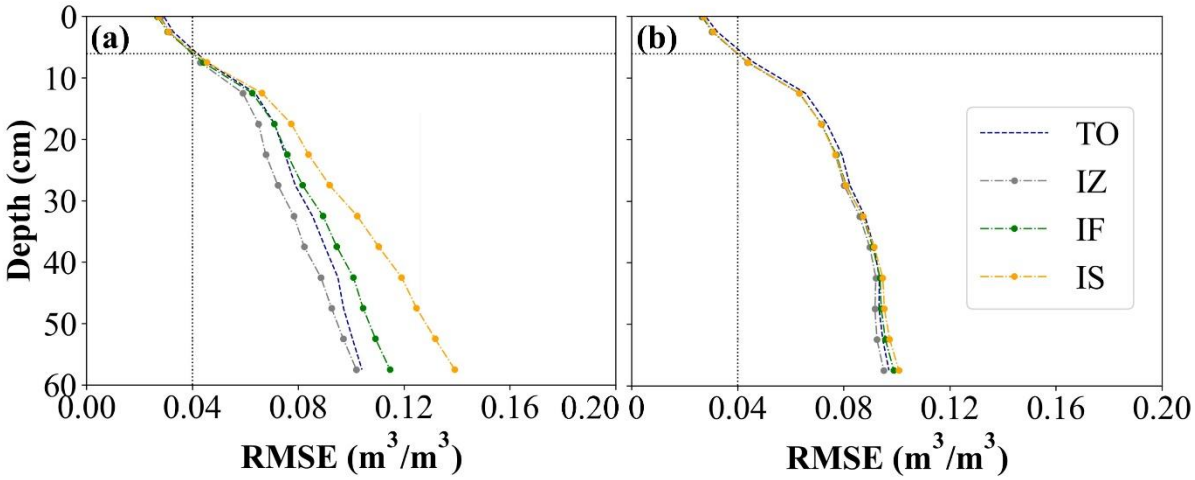

Fig. 5. Average RMSE between observed and estimated soil moisture profile as a function of depth over all the land cover conditions by utilizing the tau-omega model (TO) or multilayer incoherent model based on zero-order (IZ), first-order (IF) or incoherent solution (IS) scattering when employing the a) linear and b) second-order polynomial profile shape function. The vertical and horizontal dotted lines show the target RMSE (0.04 m^3/m^3) and the associated maximum estimation depth respectively.

could be estimated within a target RMSE) was calculated for different levels of RMSE

343 ranging from 0.01 m^3/m^3 to 0.15m^3/m^3, different incoherent models, and stratified coherent

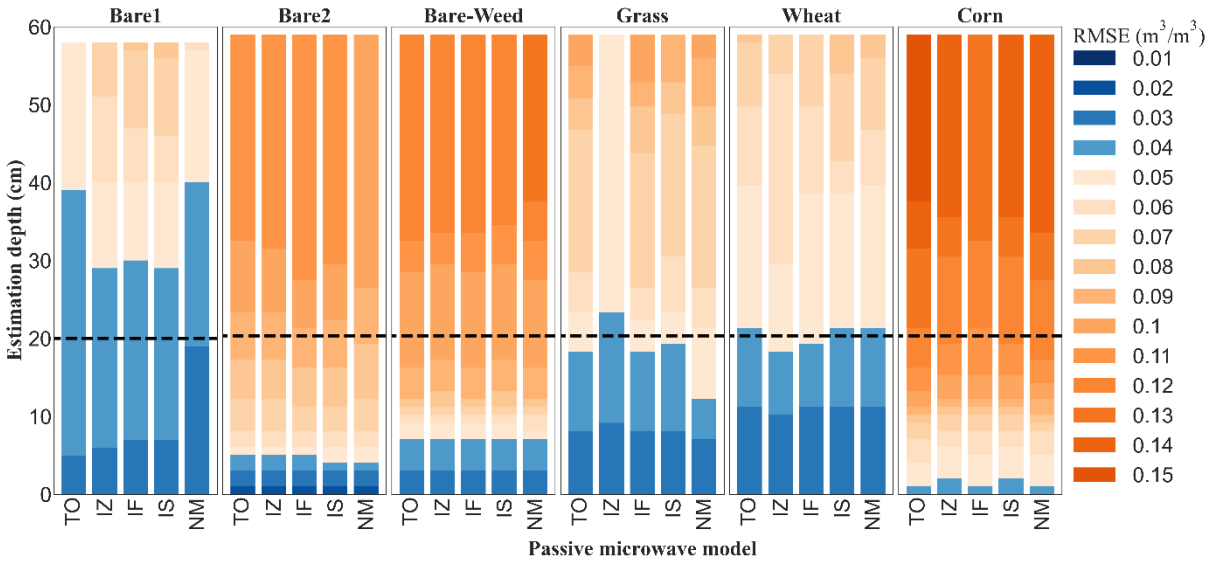

Fig. 6. Maximum estimation depth of soil moisture profile using combined L-band and P-band observations under different land cover conditions by utilizing a second-order polynomial profile shape function and employing a tau-omega model (TO), three multilayer incoherent models based on zero-order (IZ), first-order (IF), or incoherent solution (IS) scattering and the stratified coherent Njoku model (NM). The dashed line represents the 20cm estimation depth required by many applications.

model as shown in Fig. 6. The target RMSE 0.04m^3/m^3 as defined by SMOS and SMAP missions, excluding regions of frozen ground, snow and ice, open water, complex topography, urban areas, and areas with vegetation with water content greater than 5 kg/m^2, was also used as a reference here. It was found that under this target RMSE, the conventional TO model achieved an average profile estimation depth of 39cm (bare1), 5cm (bare2), 7cm (bare-weed), 18cm (grass), 21cm (wheat), and 1cm (corn). Although there are minor differences between the results of the models during dry periods, they exhibit near-identical results during wet periods such as bare 2 and bare-weed periods, with the lowest RMSE being 0.01m^3/m^3 during bare 2. As mentioned earlier, this is attributed to the shallow sensing depth of L-band and P-band frequencies during wet periods. Consequently, multi-layered and conventional models, as well as coherent and incoherent models, yield comparable results.

The stratified coherent Njoku model exhibited superiority only during bare 1 period. This can be attributed to the fact that, in the absence of vegetation and with low soil moisture content, the sensing depth of both the bands increases. As a result, stratified coherent models can surpass the performance of both conventional and multilayer incoherent models under such conditions. The slight superiority of coherent models over incoherent models for estimating brightness temperature under bare soil condition was also proved by Brakhasi et al. (2023a).

The estimation of soil moisture variation to a depth of 20cm is critical for two primary reasons. First, this zone is characterized by high variability in both the temporal and spatial domains, as noted by Shi et al. (2014). Second, the roots of major agricultural crops are primarily situated in this region, as highlighted by Haberle and Svoboda, (2015). All the employed models estimated the soil moisture profile to this depth with an RMSE of approximately $0.04 m^3/m^3$ in the periods bare1, grass and wheat. However, during bare2, bare-weed and corn periods, the RMSEs were somewhat higher, at 0.09, 0.10, and $0.12 m^3/m^3$, respectively. The lower soil moisture profile estimation depth during the corn period could be attributed to the high soil moisture (average 0.21, 0.40, and $0.31 m^3/m^3$ at depth 0-5cm, 35-40cm, and 55-60cm respectively) and its steepness near the surface, and also the high vegetation water content (average 12.5 kg/m^2 over the entire period). The evolution time series of estimated and observed soil moisture using the models is shown in Fig. 7 and Fig. 8 for depths of 0-30cm and 30-60cm respectively, in 5cm intervals. The results of the models for the surface layers show a narrow range of variation, but as the depth of the soil increases, differences between the models become more apparent. Moreover, the differences between the models during the dry periods, such as bare1, grass and wheat, are more obvious than during wet periods, such as bare2, bare-weed and corn, as depicted in Fig. 8. Except for the grass period, the models overestimated the soil moisture at the deeper layers during the dry periods and and underestimated during the wet periods.

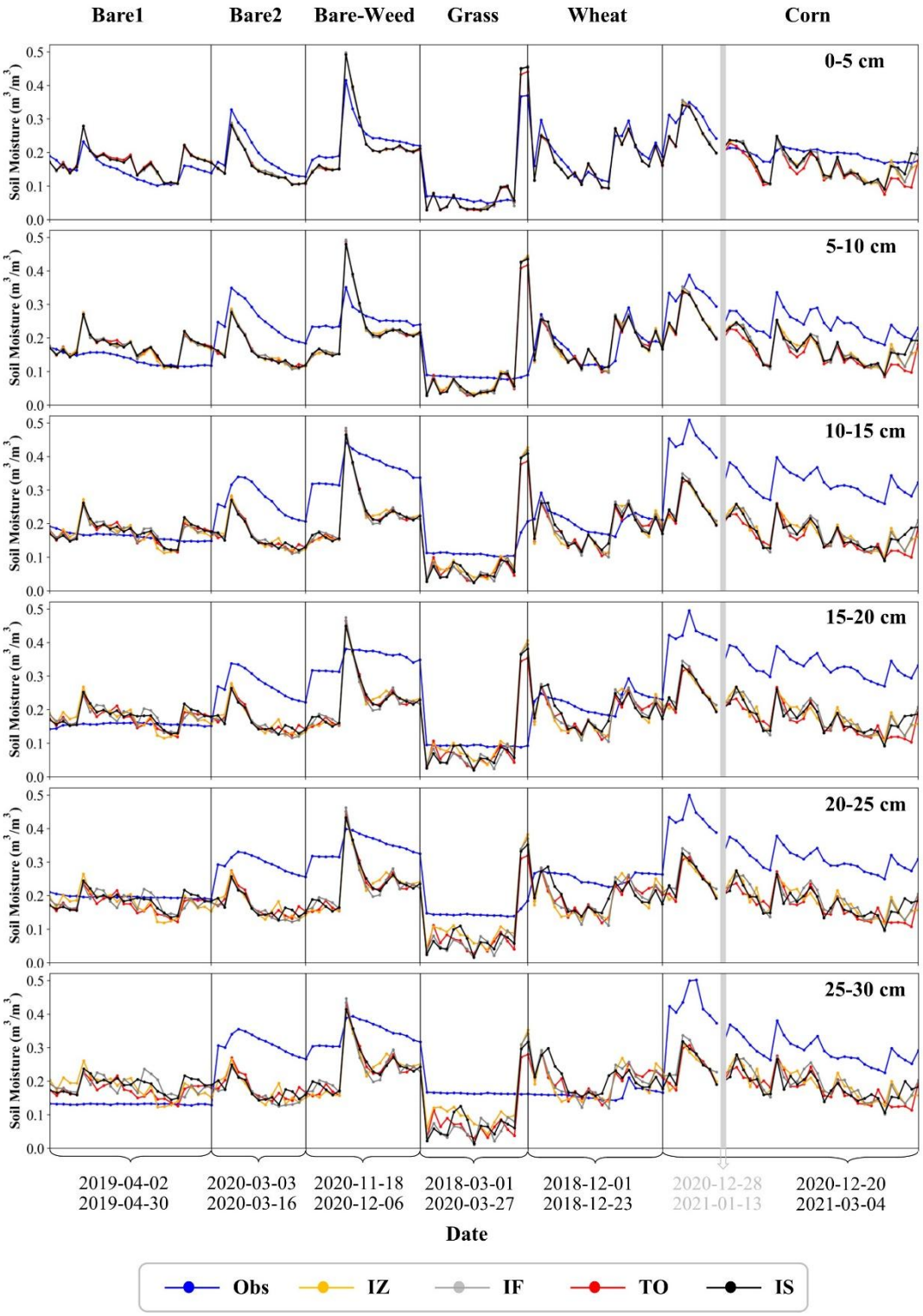

Fig. 7. Time series observations, estimated soil moisture at different depths from the surface to 30cm using four incoherent models being the tau-omega model (TO) or a multilayer incoherent model based on zero-order (IZ), first-order (IF) or incoherent solution (IS) scattering and employing a second-order polynomial profile shape function. Each row represents one depth.

380

381

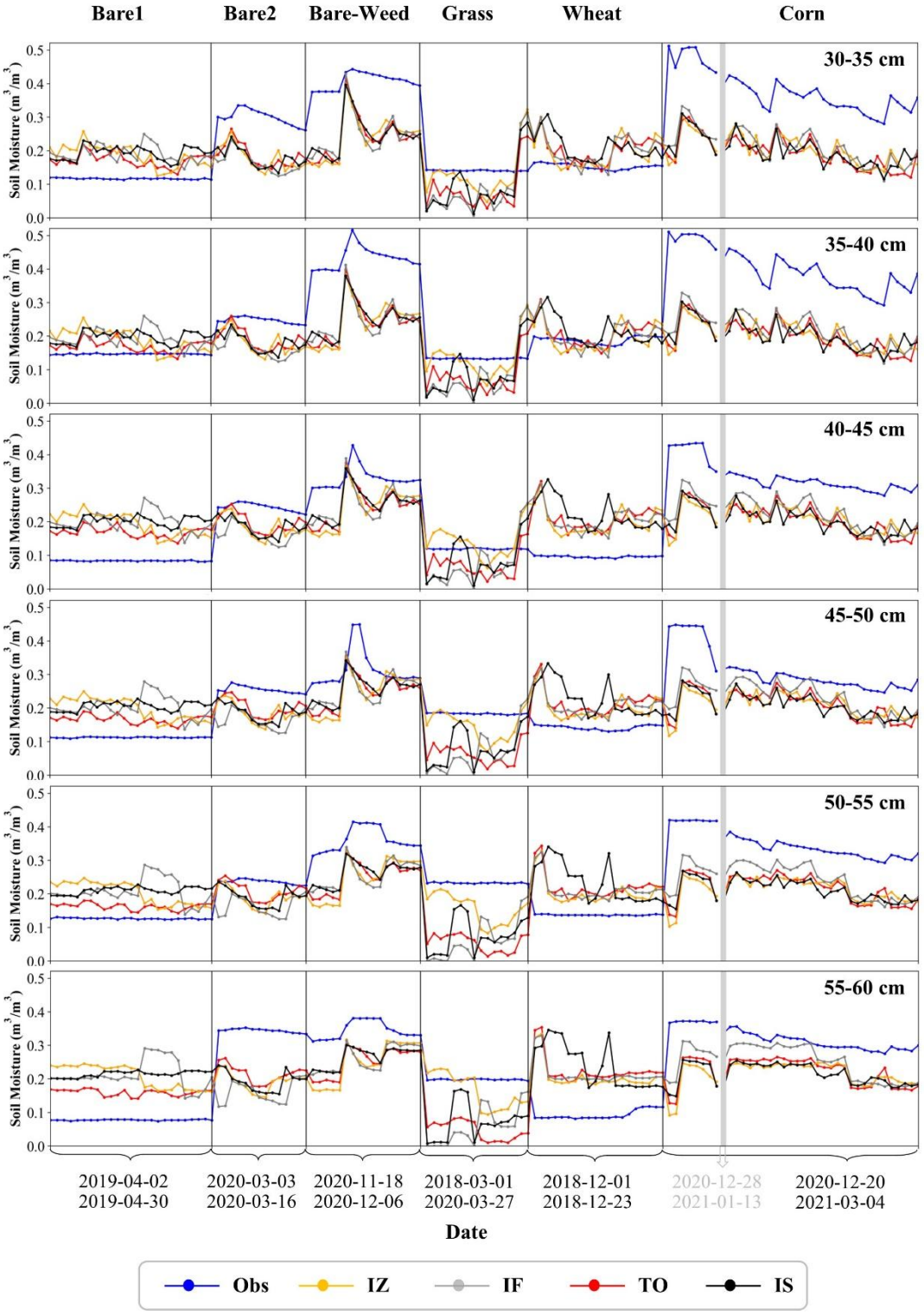

Fig. 8. As for Fig. 7 but for depths from 30cm to 60cm.

5. Conclusions

Four incoherent passive microwave models including the conventional tau-omega model (TO), and three multilayers models based on zero-order (IZ), first-order (IF) and incoherent solution (IS) scattering approximations were compared to estimate soil moisture profile. The result of these models was also compared with the stratified coherent model results of Njoku model (NM; Njoku and Kong, 1977) employed in Brakhasi et al. (2023). Observations from a tower-based experiment at Cora Lynn, Victoria, Australia under different land cover conditions (bare, bare-weed, grass, wheat, and corn) including L-band and P-band brightness temperature, soil moisture and temperature at different depths in the profile to 60cm, along with weekly measurements of vegetation water content and surface roughness were used. A time series approach was employed by combining L-band and P-band brightness temperature observations with either a linear (Li) or second-order polynomial (Pn2) profile shape function to represent the soil moisture profile variation with depth. The RMSE between observed and estimated soil moisture profiles was calculated at various depths, with the multilayer incoherent models IZ, IF, and IS having slightly better results than the conventional TO model, especially at shallow layers. However, the complexity of these multi-layer models and the additional information on soil temperature throughout the profile, was found to be unwarranted. Moreover, it was found that the Pn2 profile shape function outperformed the Li shape function in terms of accuracy and robustness, particularly at deeper layers. However, the estimation depth under the target RMSE of $0.04 m^3/m^3$ varied widely depending on the soil moisture conditions, ranging from 1cm to 39cm. Overall, the results of this study showcase the potential of integrating L-band and P-band radiometry to estimate soil moisture profile information at the global scale, utilizing incoherent models that perform just as effectively as the coherent model. This has important implications for a wide range of applications, including agriculture, climate science, and disaster management, and

demonstrates the value proposition for a combined L- and P-band passive microwave satellite mission for global soil moisture profile mapping.

Acknowledgments

This work was supported by the Australian Research Council through the Towards P-Band Soil Moisture Sensing from Space Project under Discovery Grant DP170102373, and Linkage, Infrastructure, Equipment and Facility Grants LE0453434 and LE150100047. The authors wish to thank Pascal Mater and Kiri Mason for their help with maintenance of the experimental equipment and site.

References

Baroni, G., Ortuani, B., Facchi, A., Gandolfi, C., 2013. The role of vegetation and soil properties on the spatio-temporal variability of the surface soil moisture in a maize-cropped field. J. Hydrol. 489, 148–159. https://doi.org/10.1016/j.jhydrol.2013.03.007

Brakhasi, F., Walker, J.P., Ye, N., Wu, X., Shen, X., Yeo, I.-Y., Boopathi, N., Kim, E., Kerr, Y., Jackson, T., 2023. Towards soil moisture profile estimation in the root zone using L- and P-band radiometer observations: A coherent modelling approach. Sci. Remote Sens. 7, 100079. https://doi.org/10.1016/j.srs.2023.100079

Burke, W.J., Paris, J.F., 1975. A radiative transfer model for microwave emissions from bare agricultural soils.

Burke, W.J., Schmugge, T., Paris, J.F., 1979. Comparison of 2.8- and 21-cm microwave radiometer observations over soils with emission model calculations. J. Geophys. Res. 84, 287. https://doi.org/10.1029/JC084iC01p00287

Eberhart, R., Kennedy, J., 1995. Particle swarm optimization, in: Proceedings of the IEEE International Conference on Neural Networks. Citeseer, pp. 1942–1948.

Entekhabi, D., Yueh, S., De Lannoy, G., 2014. SMAP handbook.

Fagerlund, E., Kleman, B., Sellin, L., Svensson, H., 1970. Physical studies of nature by thermal mapping. Earth-Sci. Rev. 6, 169–180.

Ferrazzoli, P., Paloscia, S., Pampaloni, P., Schiavon, G., Solimini, D., Coppo, P., 1992. Sensitivity of microwave measurements to vegetation biomass and soil moisture content: a case study. IEEE Trans. Geosci. Remote Sens. 30, 750–756. https://doi.org/10.1109/36.158869

Haberle, J., Svoboda, P., 2015. Calculation of available water supply in crop root zone and the water balance of crops. Contrib. Geophys. Geod. 45, 285–298. https://doi.org/10.1515/congeo-2015-0025

ITU, 2015. International telecommunication union recommendation: Radio noise.

Jackson, T., Kimball, J., 2009. SMAP Mission Science Issues Associated with Overpass Time. SMAP Sci. Doc.

Jackson, T.J., Schmugge, T.J., 1991. Vegetation effects on the microwave emission of soils. Remote Sens. Environ. 36, 203–212. https://doi.org/10.1016/0034-4257(91)90057-D
Kerr, Y.H., Waldteufel, P., Richaume, P., Wigneron, J.P., Ferrazzoli, P., Mahmoodi, A., Al Bitar, A., Cabot, F., Gruhier, C., Juglea, S.E., Leroux, D., Mialon, A., Delwart, S., 2012. The SMOS Soil Moisture Retrieval Algorithm. IEEE Trans. Geosci. Remote Sens. 50, 1384–1403. https://doi.org/10.1109/TGRS.2012.2184548
Lee, S.L., 1974. Dual frequency microwave radiometer measurements of soil moisture for bare and vegetated rough surfaces.
Liu, P.-W., De Roo, R.D., England, A.W., Judge, J., 2013. Impact of Moisture Distribution Within the Sensing Depth on L- and C-Band Emission in Sandy Soils. IEEE J. Sel. Top. Appl. Earth Obs. Remote Sens. 6, 887–899. https://doi.org/10.1109/JSTARS.2012.2213239
Lv, S., Wen, J., Zeng, Y., Tian, H., Su, Z., 2014. An improved two-layer algorithm for estimating effective soil temperature in microwave radiometry using in situ temperature and soil moisture measurements. Remote Sens. Environ. 152, 356–363. https://doi.org/10.1016/j.rse.2014.07.007
Ma, X., Han, F., Wu, J., Ma, Y., Jacoby, P.W., 2023. Optimizing crop water productivity and altering root distribution of Chardonnay grapevine (Vitis vinifera L.) in a silt loam soil through direct root-zone deficit irrigation. Agric. Water Manag. 277, 108072. https://doi.org/10.1016/j.agwat.2022.108072
Manoj, A., Guntu, R.K., Agarwal, A., 2022. Spatiotemporal dependence of soil moisture and precipitation over India. J. Hydrol. 610, 127898. https://doi.org/10.1016/j.jhydrol.2022.127898
Merlin, O., Walker, J.P., Panciera, R., Young, R., Kalma, J.D., Kim, E.J., 2007. Calibration of a soil moisture sensor in heterogeneous terrain, in: MODSIM 2007 International Congress on Modelling and Simulation. Modelling and Simulation Society of Australia and New Zealand. pp. 2604–2610.
Mironov, Bobrov, P.P., Fomin, S.V., 2013. Multirelaxation Generalized Refractive Mixing Dielectric Model of Moist Soils. IEEE Geosci. Remote Sens. Lett. 10, 603–606. https://doi.org/10.1109/LGRS.2012.2215574
Mladenova, I.E., Jackson, T.J., Njoku, E., Bindlish, R., Chan, S., Cosh, M.H., Holmes, T.R.H., de Jeu, R.A.M., Jones, L., Kimball, J., Paloscia, S., Santi, E., 2014. Remote monitoring of soil moisture using passive microwave-based techniques — Theoretical basis and overview of selected algorithms for AMSR-E. Remote Sens. Environ. 144, 197–213. https://doi.org/10.1016/j.rse.2014.01.013
Mo, T., Choudhury, B.J., Schmugge, T.J., Wang, J.R., Jackson, T.J., 1982. A model for microwave emission from vegetation-covered fields. J. Geophys. Res. 87, 11229. https://doi.org/10.1029/JC087iC13p11229
Njoku, E.G., 1976. Microwave remote sensing of near-surface moisture and temperature profiles. (PhD Thesis). Massachusetts Institute of Technology.
Njoku, E.G., Kong, J.-A., 1977. Theory for passive microwave remote sensing of near-surface soil moisture. J. Geophys. Res. 82, 3108–3118. https://doi.org/10.1029/JB082i020p03108
Oki, T., Kanae, S., 2006. Global Hydrological Cycles and World Water Resources. Science 313, 1068–1072. https://doi.org/10.1126/science.1128845
Paloscia, S., Pampaloni, P., Chiarantini, L., Coppo, P., Gagliani, S., Luzi, G., 1993. Multifrequency passive microwave remote sensing of soil moisture and roughness. Int. J. Remote Sens. 14, 467–483. https://doi.org/10.1080/01431169308904351
Robinson, D.A., Campbell, C.S., Hopmans, J.W., Hornbuckle, B.K., Jones, S.B., Knight, R., Ogden, F., Selker, J., Wendroth, O., 2008. Soil Moisture Measurement for Ecological

and Hydrological Watershed- Scale Observatories: A Review. Vadose Zone J. 7, 358–389. https://doi.org/10.2136/vzj2007.0143
Sadri, S., Pan, M., Wada, Y., Vergopolan, N., Sheffield, J., Famiglietti, J.S., Kerr, Y., Wood, E., 2020. A global near-real-time soil moisture index monitor for food security using integrated SMOS and SMAP. Remote Sens. Environ. 246, 111864. https://doi.org/10.1016/j.rse.2020.111864
Schoener, G., Stone, M.C., 2020. Monitoring soil moisture at the catchment scale – A novel approach combining antecedent precipitation index and radar-derived rainfall data. J. Hydrol. 589, 125155. https://doi.org/10.1016/j.jhydrol.2020.125155
Shen, X., Jeffrey, W., Nan, Y., Xiaoling, W., Foad, B., Liujun, Z., Edward, K., Yann, K., Thomas, J., 2023. Evaluation of the Tau-Omega Model over a Dense Corn Canopy at P- and L-band. Geosci. Remote Sens. Lett. Under review.
Shen, X., Walker, J.P., Ye, N., Wu, X., Boopathi, N., Yeo, I.-Y., Zhang, L., Zhu, L., 2021. Soil Moisture Retrieval Depth of P- and L-Band Radiometry: Predictions and Observations. IEEE Trans. Geosci. Remote Sens. 59, 6814–6822. https://doi.org/10.1109/TGRS.2020.3026384
Shen, X., Walker, J.P., Ye, N., Wu, X., Brakhasi, F., Boopathi, N., Zhu, L., Yeo, I.-Y., Kim, E., Kerr, Y., Jackson, T., 2022. Evaluation of the tau-omega model over bare and wheat-covered flat and periodic soil surfaces at P- and L-band. Remote Sens. Environ. 273, 112960. https://doi.org/10.1016/j.rse.2022.112960
Shi, Y., Wu, P., Zhao, X., Li, H., Wang, J., Zhang, B., 2014. Statistical analyses and controls of root-zone soil moisture in a large gully of the Loess Plateau. Environ. Earth Sci. 71, 4801–4809. https://doi.org/10.1007/s12665-013-2870-5
Stogryn, A., 1970. The Brightness Temperature of a Vertically Structured Medium. Radio Sci. 5, 1397–1406. https://doi.org/10.1029/RS005i012p01397
Svoboda, P., Raimanová, I., Duffková, R., Fučík, P., Kurešová, G., Haberle, J., 2020. The effects of irrigation on root density profiles of potato, celery, and wheat 911.1Kb. https://doi.org/10.15159/AR.20.035
Swaroop Meena, R., Datta, R. (Eds.), 2021. Soil Moisture Importance. IntechOpen. https://doi.org/10.5772/intechopen.82898
Ulaby, F.T., Moore, R.K., Fung, A.K., 1986. Microwave remote sensing: Active and passive. Volume 3-From theory to applications.
Wang, J.R., Choudhury, B.J., 1981. Remote sensing of soil moisture content, over bare field at 1.4 GHz frequency 27.
Wang, J.R., McMurtrey III, J.E., Engman, E.T., Jackson, T.J., Schmugge, T.J., Gould, W.I., Fuchs, J.E., Glazar, W.S., 1982. Radiometric measurements over bare and vegetated fields at 1.4-GHz and 5-GHz frequencies. Remote Sens. Environ. 12, 295–311.
Wigneron, J.P., Kerr, Y., Waldteufel, P., Saleh, K., Escorihuela, M.-J., Richaume, P., Ferrazzoli, P., de Rosnay, P., Gurney, R., Calvet, J.-C., Grant, J.P., Guglielmetti, M., Hornbuckle, B., Mätzler, C., Pellarin, T., Schwank, M., 2007. L-band Microwave Emission of the Biosphere (L-MEB) Model: Description and calibration against experimental data sets over crop fields. Remote Sens. Environ. 107, 639–655. https://doi.org/10.1016/j.rse.2006.10.014
Wigneron, J.-P., Laguerre, L., Kerr, Y.H., 2001. A simple parameterization of the L-band microwave emission from rough agricultural soils. IEEE Trans. Geosci. Remote Sens. 39, 1697–1707. https://doi.org/10.1109/36.942548
Wilheit, T.T., 1978. Radiative Transfer in a Plane Stratified Dielectric. IEEE Trans. Geosci. Electron. 16, 138–143. https://doi.org/10.1109/TGE.1978.294577

Xu, L., Chen, N., Zhang, X., Moradkhani, H., Zhang, C., Hu, C., 2021. In-situ and triple-collocation based evaluations of eight global root zone soil moisture products. Remote Sens. Environ. 254, 112248. https://doi.org/10.1016/j.rse.2020.112248